Femtosecond laser control of the angular distribution of electrons due to autoionization

M. L. Bajema, R. R. Jones, and T. F. Gallagher
Department of Physics, University of Virginia, Charlottesville, Virginia 22904-4714, USA
(Received 25 June 2004; published 30 December 2004)

Using two 500-fs laser pulses and a controlled time delay between them we are able to manipulate the angular distributions of the electrons ejected by autoionization of Ca atoms in the $4p_{3/2}21s$ and $4p_{3/2}19d$ states. Subsequent to their isolated core excitation by a 500-fs 393-nm laser pulse, Ca $4p_{3/2}21s(19d)$ Rydberg atoms coherently evolve, via configuration interaction, into the degenerate $4p_{1/2}ns(nd)$ states. While in the $4p_{1/2}ns(nd)$ states atoms can be de-excited to bound $4sns(nd)$ levels using a 500-fs 397-nm pulse. Removing these atoms from the autoionizing states leads to a greater fraction of electrons leaving the atom along the direction of the laser polarization than is possible through direct excitation of $4_{3/2}ns(nd)$ or $4p_{1/2}ns(nd)$ using either the 393- or 397-nm pulse alone.

DOI: 10.1103/PhysRevA.70.062722 PACS number(s): 32.80.Dz

I. INTRODUCTION

One of the original ideas for using a laser to do selective chemistry was to excite resonantly the vibrational motion of a single bond, and through the absorption of many photons reach the dissociation limit, breaking the bond [1]. This approach has proven to be unworkable with laser pulse lengths of 1 ns or longer because the vibrational modes of a molecule are coupled. Consequently, any attempt to deposit a large amount of energy into one vibrational mode is thwarted by rapid intramolecular vibrational relaxation (IVR), which redistributes the energy to other vibrations as rapidly as it is deposited in the selected mode by the laser.

The advent of mode locked lasers has provided a tool with a time resolution comparable to the ps time scale of IVR. With such lasers, together with coherence, IVR might be exploited to enable bond selective chemistry, and several different approaches have been suggested. In the first approach a ps laser excites a coherent superposition of eigenstates, which are linear combinations of the excited states of different vibrational modes [2]. The coherent superposition corresponds initially to the excitation of a single vibration. In time, the energy within the molecule flows into different vibrations. Left to itself, vibrational energy within the molecule would simply move coherently between available modes. However, to control its reactivity one can use a second, time delayed, ps laser pulse to further excite or deexcite the molecule as it samples different vibrational modes. The use of a second, time delayed, pulse allows population of molecular states completely inaccessible by direct excitation from the ground state.

The approach outlined above relies on the coherence of the quantum-mechanical states excited by the laser. An alternative approach is to use the interference between two coherent excitation pathways to achieve the desired result [3–7]. In this case, often the fundamental frequency of a laser and a phase locked harmonic are used to drive single and multiphoton transitions simultaneously. This approach has been used to control the photoionization of atoms and molecules and the photodissociation of molecules [3–7]. While conceptually attractive, this method is limited in that the magnitude of the interference, which provides the control, is determined by the weaker of the couplings, usually the multiphoton coupling. Finally, methods which depend upon both the quantum-mechanical coherence of the atom or molecule and the optical coherence of the exciting laser have been used. For example, the angular distributions of electrons ejected from atomic autoionizing states of mixed configuration have been controlled in this way [8,9].

Here we report the manipulation of the angular distribution of electrons ejected from autoionizing states of Ca, the eigenstates of which are of mixed configuration, e.g., $4p_{1/2}ns, 4p_{3/2}n's, 4s\varepsilon\ell$. This is an example of the first type of control mentioned above, that is we use two independent ps laser pulses. The first pulse creates a coherent superposition which oscillates between configurations, and the second depletes one configuration. This form of control allows us to alter the angular distribution of the ejected electrons, and with the correct choice of time delay between the two lasers we are able to produce a higher fraction of electrons ejected along the direction of the laser polarization than can be obtained by exciting either configuration alone. It has the additional attraction of using large optical cross sections, i.e., it is not limited by the weaker of interfering amplitudes, and as a result is efficient in its use of laser photons. Moreover, the differential control does not come at the expense of total yield which typically varies by only 20% as a function of the relative delay of the pump-dump control fields. In the sections which follow we describe the experimental procedure and our results, followed by an explanation of our observations.

II. EXPERIMENTAL APPROACH

In our experiment, atoms in a thermal beam of Ca from a resistively heated oven are excited first to the $4s5p$ state and then to a single $4sns$ or $4snd$ state by two narrow-band laser pulses as shown in the energy level diagram of Fig. 1. Here, we explicitly consider the population of $4s21s$ state. Atoms in the $4s21s$ state are further excited by a 500-fs 393-nm pulse to the $4p_{3/2}21s$ autoionizing state. This transition is an isolated core excitation (ICE) in which the $4s$ electron of the Ca^+ core is excited to the $4p_{3/2}$ state while the $21s$ electron

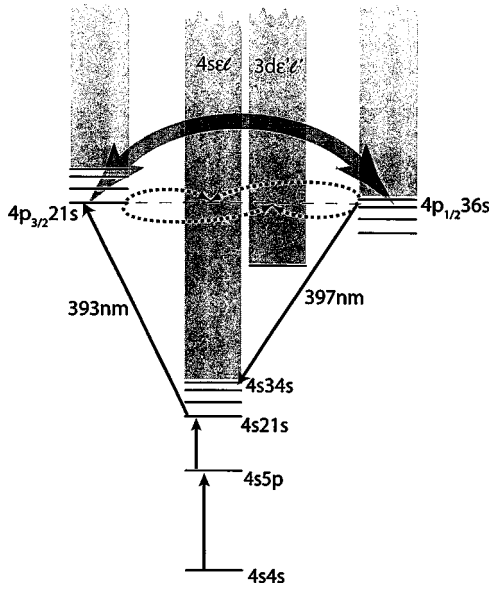

FIG. 1. Ca atoms in the ground $4s^2$ state are excited by narrow-band laser pulses at 240 nm and 1.365 μm via the $4s5p$ state to the $4s21s$ state. These atoms are exposed to a 500-fs 393-nm pulse which drives them to the $4p_{3/2}21s$ autoionizing state, which can either autoionize into the $4s_{1/2}$ or $3d_j$ continua or evolve into the degenerate $4p_{1/2}ns$ states ($n\sim36$). The 397-nm pulse comes at a variable time before or after the 393-nm pulse. If it comes immediately afterwards, so there is some amplitude in the $4p_{1/2}ns$ states, the 397-nm pulse can stimulate emission down to the bound $4sns$ levels. This bound state probability does not contribute to the observed electron angular distribution, which is significantly different from that observed with the 393-nm pulse alone. The dashed lines indicate autoionization pathways while the broad gray line denotes bound-state configuration interaction.

is, in essence, a spectator [10]. The 393-nm pulse excites a coherent superposition of energy eigenstates; each of which is composed of a different linear combination of $4p_{3/2}21s$, $4p_{1/2}ns$, and continuum configurations. The center of the $4p_{3/2}21s$ resonance has an effective quantum number $n^*=33.6$ relative to the $4p_{1/2}$ limit, and within its full width at half maximum, the $4p_{3/2}21s$ level spans the $4p_{1/2}35s$–$4p_{1/2}37s$ states. The $4p_{3/2}ns$ autoionizing states are also coupled to the Ca^+ $3d$ and Ca^+ $4s$ continua. Initially, only the $4p_{3/2}ns$ configuration is present, but as time evolves it disappears and the others appear. At a variable time, usually after the 393-nm pulse, the atoms are exposed to a 397-nm pulse, which is at the frequency of the Ca $4s_{1/2}$–$4p_{1/2}$ transition. If this 397-nm pulse comes before the 393-nm pulse it excites the $4s21s$ atoms to the $4p_{1/2}21s$ state instead of the $4p_{3/2}21s$ state, and they simply autoionize. If it comes after the 393-nm pulse and the atoms initially in the $4p_{3/2}21s$ state have evolved into the $4p_{1/2}ns$ states, it can drive atoms down to the bound $4s_{1/2}ns$ states. By detecting the bound $4sns$ atoms it is possible to make a time-resolved measurement of the population in the $4p_{1/2}ns$ states as shown in Fig. 2. Similar measurements were made previously by Ereifej and Story [11] who detected the "stairstep decay" predicted by Wang and Cooke [12]. The "stairstep decay" has now been detected in several contexts [13–15].

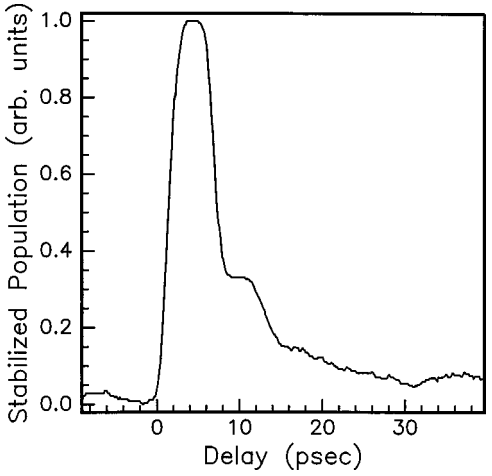

FIG. 2. Bound-state $4sns$ signal as a function of delay between the 393- and 397-nm laser pulses. The 393-nm pulse drives the isolated-core excitation of the $4p_{3/2}21s$ atoms and the 397-nm laser pulse de-excites and stabilizes $4p_{1/2}ns$ population resulting from configuration interaction. Within 1 ps of the initial excitation, 90% of the initial $4p_{3/2}21s$ population has decayed via autoionization or has been transferred to a $4p_{1/2}ns$ radial wave packet. The wave-packet population decays in a series of stairsteps since autoionization can only occur at times when the Rydberg electron is near the ion core. Using our technique we can only detect those atoms which are in the $4p_{1/2}ns$ states. This population is never more than 20% of the population initially excited to the $4p_{3/2}21s$ state.

We detect the angle and energy resolved electrons as a function of the delay between the 393- and 397-nm laser pulses. The controlling effect of the 397-nm laser is to remove probability amplitude which has evolved from the $4p_{3/2}21s$ state to the $4p_{1/2}ns$ states, so that this amplitude does not contribute to the outgoing continuum electron wave packet.

All the optical pulses are derived from an amplified, mode-locked titanium sapphire laser operating at $\lambda=790$ nm with a 120-fs pulse length. These pulses are amplified to 2 mJ at a 1-kHz repetition rate, and 90% of the output is used to pump optical parametric amplifiers that enable the generation of light at 240 nm and 1.365 μm, to drive the first two transitions shown in Fig. 1. The remaining 10% of the 790-nm light is split into two beams which are doubled in two, 1-cm-long KDP crystals to generate the 500-fs 393-nm and 397-nm pulses. The phase matching constraint of the KDP doubling crystals, angle tuned to produce 393 and 397 nm, leads to the production of spectrally narrower (~30 cm^{-1})500-fs pulses. This bandwidth is much less than the Ca^+ $4p_{1/2}$-$4p_{3/2}$ fine-structure splitting of 222 cm^{-1}, so we estimate that the 393- (397-)nm light excites negligible amounts of $4p_{1/2}n\ell$ ($4p_{3/2}n\ell$) population. The 397-nm pulse passes through an optical delay line which allows us to vary its arrival at the atomic beam from 10 ps before the 393-nm pulse to 50 ps after it. All of the four beams are linearly polarized in the same direction.

The ejected electrons are detected by a dual microchannel plate located 25 cm from the point where the laser beams cross the atomic beam. The resolution in the angle θ at which the electrons are ejected relative to the laser polarization is

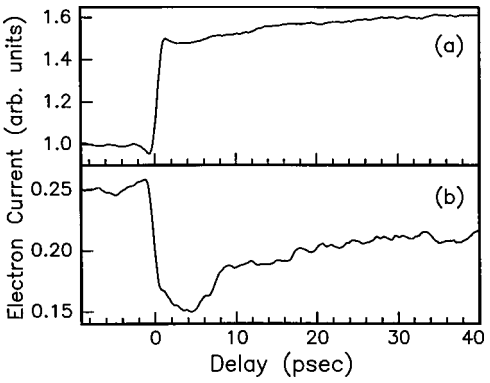

FIG. 3. Integrated lock-in data obtained using the $4s21s$ state showing the 3.1-eV electrons ejected (a) along the laser polarization ($\theta=0$) and (b) perpendicular to the laser polarization ($\theta=90°$) vs time delay t of the 397-nm pulse. For $t\sim-10$ ps the primary excitation is by the 397-nm pulse and for $t\sim40$ ps it is by the 393-nm pulse. The region $0<t<20$ ps shows the effect of removing probability amplitude which has evolved from the $4p_{3/2}21s$ state to the $4p_{1/2}ns$ levels.

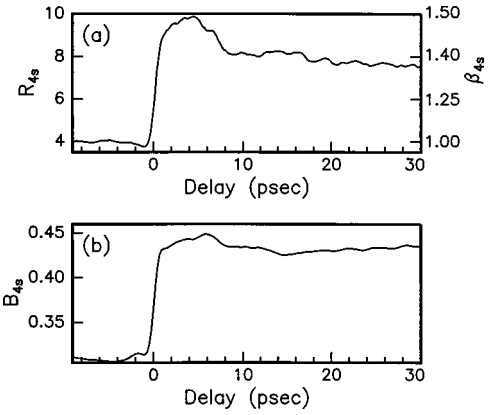

FIG. 4. (a) R_{4s}, the ratio of the number of 3.1-eV electrons ejected at 0° to the number ejected at 90° vs time delay t of the 397-nm pulse for the $4s21s$ state. On the right-hand side of the figure R_{4s} is expressed in terms of the β parameter. (b) B_{4s}, the branching ratio for 3.1-eV electrons vs t. Note that in both cases for $t\sim5$ ps the values are higher than obtained for either 393- or 397-nm light alone.

7° and the energy resolution is 0.5 eV, sufficient to separate the 3.1-eV electrons ejected in autoionization to the Ca^+ $4s$ state from the 1.5-eV electrons created by autoionization to the Ca^+ $3d_j$ states. The energy resolution is not, however, adequate to discriminate between autoionization to the $3d_{3/2}$ and $3d_{5/2}$ states of Ca^+. The detector is fixed in position, and to vary θ we simultaneously rotate the polarizations of all four lasers.

Since our main interest is in determining the change in the ejected electron spectra as the time delay between the 393- and 397-nm pulses is varied, we used a lock-in detection technique. Specifically, we dithered the delay by ±1.2 ps by wobbling a glass plate in the 397-nm beam at a 71-Hz rate. The signals from the 3.1- and 1.5-eV electrons from each shot of the laser were detected with two gated integrators, and the outputs of the two integrators were used as inputs for two lock-in amplifiers. The lock in signals provided the derivatives of the 3.1- and 1.5-eV electron signals vs delay and, when integrated, were of substantially higher quality than the data obtained by simply recording the electron signals vs delay.

III. OBSERVATIONS

Typical examples of our data are shown in Fig. 3, in which we show the integrated lock in signals for the 3.1-eV electrons vs time delay t of the 397-nm pulse obtained with the first two lasers tuned to excite the $4s21s$ state. The signals shown are the total electron yields, i.e., those obtained using both lasers. In Fig. 3(a) we show the signal obtained with $\theta=0$, i.e., the electrons ejected along the laser polarization direction. For $t<0$ the 397-nm light comes before the 393-nm light and the atoms are nearly all (>80%) excited to the $4p_{1/2}21s$ state which simply autoionizes, yielding a signal of 1.0. For $t>0$ the 393-nm light comes first and nearly all the atoms are excited to the $4p_{3/2}21s$ state. For $t>40$ ps the 397-nm light arrives after all the atoms initially excited to the $4p_{3/2}21s$ have autoionized and has no effect on any of these atoms. In this case the detected signal is 1.6. There is a sharp change in the signal at $t=0$, and it slowly approaches the $t>40$-ps signal. The difference between the $0<t<30$-ps and the $t>40$-ps signal is due to the fact that some of the atoms in the initially populated $4p_{3/2}21s$ state have evolved to the degenerate $4p_{1/2}ns$ states and are driven down to the bound $4sns$ states by the 397-nm pulse.

In many ways Fig. 3(a) is what one might expect; $t=-10$ ps and +40 ps correspond, respectively, to predominantly (>80%) $4p_{1/2}21s$ and $4p_{3/2}21s$ excitations, and the region near $t\sim0$ is an interpolation between the two extremes. Figure 3(b), obtained by detecting the 3.1-eV electrons at $\theta=90°$, does not, however, fit this intuitive picture. As shown, for $t<0$ the signal is 0.25 and at $t>40$ ps it is 0.21. At $t=0$ the signal drops to 0.15, below the $t>40$-ps signal, and approaches it in steps, near $t=8$ and 17 ps.

The principal quantity we are controlling with the pair of laser pulses is the direction in which the electrons are ejected. However, as shown in Fig. 2, the total number of electrons produced varies as a function of time delay. Therefore we consider R_{4s}, the ratio of the numbers of 3.1-eV electrons ejected by autoionization to the Ca^+ $4s$ ion at 0° and 90° vs delay. This ratio is independent of the total autoionization yield. Combining the data of Figs. 3(a) and 3(b) we plot the delay dependence of R_{4s} in Fig. 4. As shown, $R_{4s}=4.0$ for $t<0$, rises to $R_{4s}=10.0$ for $0<t<8$ ps, and then falls to $R_{4s}=7.7$ for $t=40$ ps. In other words, with the 397-nm pulse delayed by ~6 ps from the 393-nm pulse we are able to produce a higher fraction of electrons ejected along the polarization direction than with either pulse by itself. In Fig. 4(a) we have on the right-hand side expressed the result in terms of the parameter β normally used to characterize photoelectron angular distributions. In particular, the electron angular distribution is described by [16]

$$I(\theta)=I_0[1+\beta P_2(\cos\theta)], \tag{1}$$

where I_0 is a constant, and $P_2(\cos\theta)$ is the Legendre polynomial. $\beta=-1$ corresponds to an $I(\theta)=\sin^2\theta$ distribution and

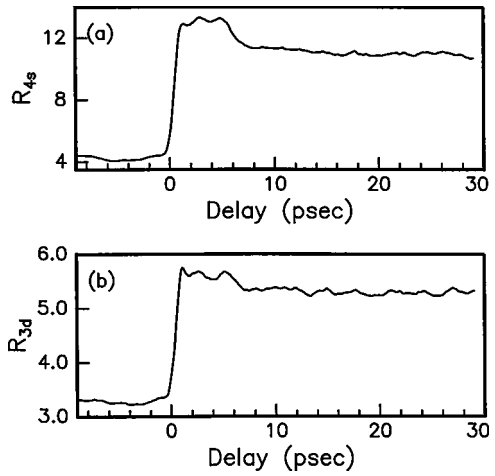

FIG. 5. Ratios of the $\theta=0°$ and $\theta=90°$ signals obtained using the 4*s*19*d* state (a) for 3.1-eV electrons, R_{4s}; and (b) 1.5-eV electrons, R_{3d}, vs *t*. Note that the values for $t\sim 5$ ps are higher than obtained with only 393- or 397-nm pulses.

$\beta=2$ corresponds to an $I(\theta)=\cos^2\theta$ distribution. In these terms β changes from 1.0 to 1.48 to 1.38 as *t* goes from -10 to 5 to 40 ps.

Shown in Fig. 4(b) is the branching ratio B_{4s} for autoionization to the 4*s* state of Ca^+. We define the branching ratio in the usual way. For example, B_{4s} is the fraction of the electrons due to autoionization to the Ca^+ 4*s* state, i.e., $B_{4s} \equiv I_{4s}/(I_{4s}+I_{3d})$. It shows a behavior similar to that seen in Fig. 4(a). For $t<0$ $B_{4s}=0.31$, for $t\rightarrow\infty$ $B_{4s}=0.43$, and for $0<t<30$ ps $B_{4s}=0.45$. Thus for both the angular distribution and the branching ratio the values for $0<t<30$ ps fall outside the range of values spanned by excitation of the $4p_{3/2}21s$ and $4p_{1/2}21s$ states alone.

The data shown in Figs. 3 and 4 are not anomalous; similar observations were made starting from the 4*snd* states. For example, in Fig. 5 we show the ratio of the $\theta=0°$ and 90° electron signals vs delay of the 397-nm pulse obtained when starting from the 4*s*19*d* state. As shown by Fig. 5(a), for $t<0$ R_{4s} is 4.3 but for $0<t<6$ ps $R_{4s}=12.8$, greater than the value $R_{4s}=10.9$ at $t>20$ ps. For $t<0$ $R_{3d}=3.3$, for $0<t<6$ ps $R_{3d}=5.6$, and it falls to 5.3 for $t>20$ ps. As in Figs. 3 and 4, the values of R_{4s} and R_{3d} obtained for $0<t<6$ ps are larger than the values for $t=-10$ ps or $t>20$ ps, and once again the large values for $0<t<6$ ps are due to depopulating the $4p_{1/2}nd$ states.

IV. DISCUSSION

To understand our results we begin by constructing the zeroth-order energy-level diagram shown in Fig. 6. It consists of the $4p_{3/2}21s$ state, several $4p_{1/2}ns$ states, and the continua. Due to the interactions between these configurations, at any energy the eigenstates are linear combinations of $4p_{3/2}ns$, $4p_{1/2}ns$, and continua. The coupling between the $4p_jns$ states and the continua leads to autoionization and broadening of the nominally bound states. Due to the interaction between the $4p_{3/2}ns$ and $4p_{1/2}ns$ series, both direct and through the continua, the more closely spaced and narrower

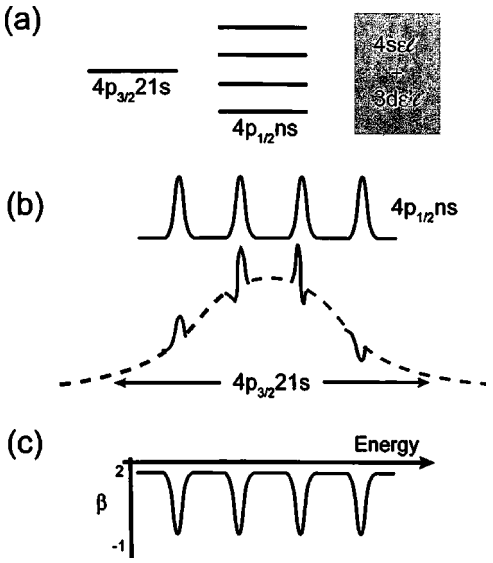

FIG. 6. (a) Zeroth-order energy-level diagram showing the $4p_{3/2}21s$ state, the $4p_{1/2}ns$ states, and the continua. (b) With the configuration interaction added the nominally bound states broaden and interact. If the $4p_{3/2}21s$ state only interacted with the continuum it would have the structure shown by the dashed line. The interaction with the $4p_{1/2}ns$ states both adds structure to the photoionization cross section shown by the solid line and produces the dips in the β parameter shown in (c).

$4p_{1/2}ns$ states impose structure on the broad photoionization feature of the $4p_{3/2}21s$ state [17,18]. The coupling between these two series has perhaps its most profound effect on the angular distributions of the electrons ejected by autoionization. In particular, the measurements of Lange *et al.* show that when the $4p_{3/2}ns$ states are excited and the angular distributions of the ejected electrons observed, there are pronounced dips in β at the locations of the $4p_{1/2}ns$ states, as shown schematically in Fig. 6(c) [19,20]. These dips are produced by interfering autoionization paths, from $4p_{3/2}21s$ and $4p_{1/2}ns$ into the degenerate continua.

Quantum defect theory calculations of the electron angular distributions and branching ratios for the Ca $4p_jns$ states have carried out using *ab initio R* matrix parameters, and the results provide a good description of the experiments [9,19,21,22]. A particular attraction of the *R*-matrix approach is that the squares of the matrix elements coupling bound to continuum channels give the partial autoionization rates, from which the branching ratios are easily computed [23].

While a quantitative theoretical description of our results might be obtained using *ab initio R* matrix parameters and quantum defect theory, we can use the qualitative resonance profile and β parameter variations shown in Figs. 6(b) and 6(c) to construct a semiclassical wave-packet picture which explains the variation in the angular distributions vs time delay [24]. At $t=0$ the ICE excitation produces atoms in the $4p_{3/2}21s$ state. If the 21*s* electron is near the Ca^+ $4p_{3/2}$ core, it can scatter superelastically to produce a $4s_{1/2}$, $3d_j$, or $4p_{3/2}$ ion. After the 1-ps Kepler orbit period for the 21*s* electron, all of the probability amplitude has had sufficient time to sample the ion core, and 90% of the electron density has coherently scattered into the degenerate continua or $4p_{1/2}ns$

states. The continuum portion represents autoionization, and the exiting electron becomes part of the observed angular distribution. Probability amplitude transferred to the $4p_{1/2}ns$ configuration leaves the nucleus as a radial wave packet, makes a complete Kepler orbit in 6 ps and returns to the ion core. Here it may scatter directly into the continua or back into the $4p_{3/2}21s$ state which, in turn, rapidly autoionizes. These two paths into the continuum interfere, and any ejected electrons become part of the observed angular distribution. If, however, the 397-nm laser de-excites the $4p_{1/2}$ core electron prior to the 21*s* wave packet's return to the nucleus, then the wave packet will not autoionize and the total electron yield and angular distribution are determined solely by the initial $4p_{3/2}21s$ decay.

Re-examining Fig. 6(c) in the light of this picture, we see that the narrow dips in the β parameter at the locations of the $4p_{1/2}ns$ states are due to the interfering amplitudes of direct and indirect autoionization upon the return of the $4p_{1/2}ns$ radial wave packet from its 6*ps* orbit. Stated another way, electrons produced via prompt autoionization of the $4p_{3/2}21s$ state have a higher β parameter than those produced by the interfering direct and indirect decay paths from the $4p_{1/2}ns$ wave packet. If the $4p_{1/2}ns$ wave packet is stabilized via stimulated emission to the 4*sns* configuration, we effectively remove the dips from the energy-dependent β parameter. Thus the β parameter we observe, which is the weighted average across the entire $4p_{3/2}21s$ profile, must rise. Stated in a slightly different way, at delay times from 0 to 6 ps the 397-nm light removes probability amplitude from the $4p_{1/2}ns$ states. This population would normally lead to lower β parameters. Consequently in this range of delay times the observed β parameter of Fig. 4(a) (or the *R* plots of Fig. 5) is higher than those observed with either 393- or 397-nm light alone.

Finally, it is useful to compare the control of the product angular distributions reported here to that reported in other work. Figure 4(a) shows that at long delay times R_{4s}, the ratio of the number of electrons emitted parallel to perpendicular to the laser polarization is 7.5. This is essentially the result from 393-nm light alone. With a delay time between zero and 6 ps we observe $R_{4s}=9.5$. In other words we have increased the ratio by 25% over what can be achieved with 393-nm light alone. Yin *et al.* [5] observed the angular distribution of photo electrons from Rb exposed to phase related linearly polarized 280- and 560-nm light. With the optimum relative phase they observed a 4:1 ratio in the number of electrons emitted in and opposite to the maximum field direction. It is convenient to term these two signals the forward and backward signals, and using these terms their result is a ratio of 4:1 for the forward and backward signals for the optimum choice of relative phase between the two harmonics. This change is much larger than we have observed, but the price is that the single photon amplitude must be reduced to match the two-photon amplitude.

Control of the product angular distributions has also been achieved at high laser intensities where different order processes often have comparable amplitudes at similar light intensities. Schumacher *et al.* [25] have examined the angular distributions of electrons from above threshold ionization of Xe by phase related 532- and 1064-nm light. With the optimum phase they observed ratios of roughly 10:1 for electrons ejected in the forward and backward directions. Sheehy *et al.* [26] observed a ratio of 1.3:1 for the forward and backward ejection of H^+ and D^+ from HD^+ when photodissociated by intense phase related 527- and 1054-nm pulses. In sum, substantial control can be exercised using intense laser fields, but it is more a characteristic of the intense fields than the atom or molecule under study.

V. CONCLUSION

Using two fs laser pulses we have demonstrated coherent control of the angular distribution of electrons ejected from doubly excited autoionizing states. Specifically, we are able to produce angular distributions more peaked along the laser polarization direction than is possible with either ps laser alone. We present a semiclassical wave-packet picture that identifies the control mechanism and qualitatively explains our results.

ACKNOWLEDGMENT

This work has been supported by the National Science Foundation through Grant Nos. PHY-0244320 and PHY-0355257.

[1] N. Bloembergen and A. H. Zewail, J. Phys. Chem. **88**, 5459 (1984).
[2] D. J. Tanner and S. A. Rice, Adv. Chem. Phys. **70**, 41 (1988).
[3] B. Sheehy, B. Walker, and L. F. DiMauro, Phys. Rev. Lett. **74**, 4799 (1995).
[4] L. Zhu, K. Suto, J. A. Fiss, R. Wada, T. Seideman, and R. J. Gordon, Phys. Rev. Lett. **79**, 4108 (1977).
[5] Y.-Y. Yin, C. Chen, D. S. Elliott, and A. V. Smith, Phys. Rev. Lett. **69**, 2353 (1992).
[6] F. Wang, C. Chen, and D. S. Elliot, Phys. Rev. Lett. **77**, 2416 (1996).
[7] S. T. Pratt, J. Chem. Phys. **104**, 5776 (1996).
[8] R. van Leeuwen, M. L. Bajema, and R. R. Jones, Phys. Rev. Lett. **82**, 2852 (1999).
[9] R. van Leeuwen, K. Vijayalakshmi, and R. R. Jones, Phys. Rev. A **63**, 033403 (2001).
[10] W. E. Cooke, T. F. Gallagher, S. A. Edelstein, and R. M. Hill, Phys. Rev. Lett. **40**, 178 (1978).
[11] H. N. Ereifej and J. G. Story, Phys. Rev. A **62**, 023404 (2000).
[12] X. Wang and W. E. Cooke, Phys. Rev. Lett. **67**, 976 (1991).
[13] J. E. Thoma and R. R. Jones, Phys. Rev. Lett. **83**, 516 (1999).
[14] S. N. Pisharody and R. R. Jones, Phys. Rev. A **65**, 033418 (2002).
[15] J. B. M. Warntjes, C. Wesdorp, F. Robicheaux, and L. D. Noordam, Phys. Rev. Lett. **83**, 512 (1999).
[16] C. N. Yang, Phys. Rev. **74**, 764 (1948).

[17] F. Gounand, T. F. Gallagher, W. Sandner, K. A. Safina, and R. Kachru, Phys. Rev. A **27**, 1925 (1983).
[18] W. E. Cooke and C. L. Cromer, Phys. Rev. A **32**, 2725 (1985).
[19] V. Lange, U. Eichmann, and W. Sandner, J. Phys. B **22**, L245 (1989).
[20] V. Lange, Ph.D. thesis, Universität Freiburg.
[21] C. H. Greene and L. Kim, Phys. Rev. A **36**, 2706 (1987).
[22] L. Kim and C. H. Greene, Phys. Rev. A **36**, 2706 (1987).
[23] W. E. Cooke and C. H. Cromer, Phys. Rev. A **32**, 2725 (1985).
[24] D. W. Schumacher, D. I. Duncan, R. R. Jones, and T. F. Gallagher, J. Phys. B **29**, L397 (1996).
[25] D. W. Schumacher, F. Weihe, H. G. Muller, and P. H. Bucksbaum, Phys. Rev. Lett. **73**, 1344 (1994).
[26] B. Sheehy, B. Walker, and L. F. DiMauro, Phys. Rev. Lett. **74**, 4799 (1995).